The Red Admiral butterfly's living light sensors and signals

Primož Pirih[1], Andrej Meglič[2], Doekele Stavenga[3], Kentaro Arikawa[4], Gregor Belušič[5]

Faraday Discussions

ROYAL SOCIETY OF CHEMISTRY

Supplementary information

1. ORG Setup, stimulation protocols and image analysis

2. Fourier domain analysis of the ommatidial eyeshine

3. SVD decomposition and clustering of pupil response spectra

1 Department of Biology, University of Ljubljana and Votan d.o.o. Ljubljana, Slovenia. Correspondence: primoz.pirih@gmail.com
2 Eye Hospital, University Medical Centre Ljubljana, Slovenia
3 Surfaces and thin films, Zernike Institute for Advanced Materials, University of Groningen, the Netherlands
4 Laboratory of Neuroethology, Sokendai – The Graduate University for Advanced Studies, Hayama, Japan
5 Department of Biology, University of Ljubljana, Slovenia

1. ORG Setup, stimulation protocols and image analysis

The telemicroscope (see Figure 4 in the main text)

Illumination in the setup is supplied by two sources. The adaptation beam consists of a collimated xenon lamp (**xbo**), shutter (**shu**), neutral density filter wedge (**f0**), bandpass filter (**f1**), light guide (**lg**), and linear polarizer (**pol**). The test beam is a collimated white LED (**led**) with an optional long-pass filter (**f2**). A coverslip (**m1**) combines the adaptation beam and test beam. The stops (**d1-d3**) correspond to the conjugated planes of the far field, cornea and eye centre, respectively. Stop (**d3**) is imaged by the telescopic pair (**l2, obj**) to the microscope objective's front focal plane (**ffp**). The back focal plane (**bfp**) of the objective is conjugated with the far field (∞**,d1**).

The eye's optical centre, the so-called deep pseudopupil (**dpp**) is then placed in the plane (**ffp**) for optimal imaging. The reflected beam, emerging from the eye is deflected by a half-mirror (m2), focussed by lens **l3** onto spatial filter **d4**, then collimated by lens **l4** and split by half-mirror **m3**. The side beam with a spectral filter **f3**, lens **l5** and monochrome camera (**bw**) is used for measurements. The vertical beam is passed to a photomicroscope for visualization of the eyeshine images and taking colour images (**rgb**).

The eye is positioned so that the eye's deep pseudopupil is imaged in the centre of the stop (**d4, Fig. 3b**). The mechanical stage with three Cartesian and two rotational degrees of freedom is allowed to settle before final readjustments. Keeping a constant temperature in the experimental room allows day-long experiments without any significant image drift.

Optical components

Filter **f0** - wedge OD [2..0], or discrete filters OD [0:1:5]. Filterbank **f1** - discrete bandpass filters [350:10:380, 400:20:700] nm, FWHM 20 nm. Filter **f2** - empty or long-pass >580 nm. Filter **f3** - bandpass 600 nm, FHWM 10 nm. Transmittance of beam splitters - **m1** 95%, **m2** 70%, **m3** 50%. Focal lengths of lenses **l1** to **l6** - 80, 60, 60, 40, 40, 20 mm, respectively; most lenses are NUV achromats (Edmund Optics). Objective **obj** - Olympus LUCplanFLN 20× NA 0.45. Cameras: **bw** - Flea3 (3.2 MP, CMOS IMX036, FLIR), **rgb** - Chameleon3 (CMOS IMX264, FLIR). Light guide **lg** - High OH 1 mm, NA 0.40 (Thorlabs).

Reducing ellipticity

The light reflected from the tapetum has a modified polarisation state due to form dichroism of the microvilli and due to the rhabdomeric waveguide effects. An optical system for studying ommatidial optics could ideally use an unpolarized test light source and polarization-insensitive detectors, but this is very difficult to build in practice. After some trial and error, we have experimentally determined the optical components and their orientation that minimized the interplay of ellipticity of dielectric beamsplitters and the dichroism of ommatidia. The LED test beam is in the horizontal plane, the illumination path is straight and the deflected main observation path is additionally rotated in the horizontal plane (**Fig. 4a**)

Calibration

We used an irradiance-calibrated spectrometer (Flame, OceanOptics, Dunedin, USA) to adjust the intensity of the adapting light beam coming through the objective in the wavelength range 350 nm

to 700 nm. The uniformity of the far field illumination of both sources was checked with a white screen behind the objective and recorded on the camera using a mirror in the front focal plane.

Stimulation protocols

Test flashes for pupil measurements were provided by a white LED source and images were taken through a 600 nm bandpass filter with a monochrome camera using 2×2 pixel binning, exposure 200 ms and gain 10 dB. Spectral adaptation light was provided by the XBO lamp, narrowband interference filters and a combination of ND grey wedge and discrete ND grey filters.

1. Spectral sensitivity of the intact eye

We first measured the pupil spectral sensitivities in the intact, unbleached eye. After each monochromatic adapting light pulse, the white LED was flashed and an image of the eyeshine reflection was taken. Images were acquired in quadruplets: a dark-adapted image was followed by three images where the pupil was activated by a sequence of 10 second pulses of linearly polarized (LP) light with diagonal (D), vertical (V) and horizontal (H) orientations, relative to the dorso-frontal eye axis. Further analysis of response curves obtained with DLP stimuli was omitted as the curves were between those obtained with VLP and HLP stimuli.

2. Intensity-response curve

Pupil responses to an intensity ladder of green (560 nm), 15 second DLP pulses with intensity increasing in 0.25 log steps were measured.

3. Polarisation sensitivity

We used blue (440 nm) LP adapting light to assess polarisation sensitivity of the pupil. A UV-capable linear polariser was rotated between horizontal orientations ψ = [– 90° +90°], obtaining 18 images with 10° steps.

4. Bleaching

The central part of the eyeshine was then selected with the cornea stop (d2, **Fig. 3b**) and subjected to a bleaching protocol where LED flashes (2 s), long-pass filtered at 580 nm, were administered four times per minute for several hours. In the first ~30 minutes, dimming of the eyeshine was observed, likely due to prolonged pupil activation. Subsequently, eyeshine reflections brightened as the concentration of green rhodopsin fell (**Fig. S1b**). The process reached a quasi-steady state after 3~4 hours. The reduced concentration of green rhodopsin also induced a change in the eyeshine reflectance colour from orange to white (**Fig. 1b**). The reflectance at 500 nm in the bleached eye part, compared to the intact part, became ~20 times higher (**Fig. S1c**).

5. Spectral sensitivity of the bleached eye

The protocol was essentially the same as for spectral sensitivity in the intact eye, except that the test LED flashes were long-pass filtered in order to sustain the bleached, low green rhodopsin state of the eye, and that the spectral sensitivity was measured in the shortened range from 350 nm to 600 nm.

6. Static eyeshine

After completing the measurements, static reflection images and RGB images were with monochromatic light between 400 and 700 nm. The ND wedge was adjusted so that the images were not overexposed. The reflectance ratio between bleached and intact ommatidia (**Fig. S1c**) was calculated from ROIs in the same images, so white reference images were not needed.

7. Recovery from bleaching

The eye was left to recover almost completely for about 2 hours and control images were taken every 10~30 minutes (**Fig. S1d**).

8. Instrumental background

Finally, the animal was removed and a series of background images containing faint lens reflections were acquired, averaged and subtracted from the eyeshine image stacks during image analysis.

Image analysis

Stack preparation

The stacks with eyeshine images acquired with the stimulation protocols (**Fig. S1a**) were imported into Fiji/ImageJ, corrected for the background and registered to the reference image using plugins bUnwarpJ and StackReg. The centres of ommatidia in the reference image were found using the function “Find Peaks”. After adding missing peaks and removing double peaks, Voronoi segmentation was performed with the function “Analyse particles” to obtain regions of interest (ROIs). After excluding some dust-covered ommatidia, the mean grey value data from 628 ommatidia from the central area were exported to GNU Octave and converted to log reflectance values using dark-adapted reference grey values from the same ROIs. The ROI lattice is shown in **Fig. 5**.

Calculation of log reflectance and normalisation

Mean values of ROIs were converted to log reflectance change as $A_{mn} = -\log_{10}(g_{mn}/g_{mn0})$, where g_{mn} is the reflectance value of the m^{th} ommatidium in the n^{th} image, and g_{mn0} is the dark-adapted reference obtained immediately before (**Fig. S1a**). We noticed that while the absolute magnitudes of pupil spectra were different, their shapes were consistent. We therefore normalised the log reflectance spectra to equal response area separately for each ommatidium and separately for the intact and bleached experimental runs (**Fig. 6a**).

Polarisation sensitivity analysis

The linear polariser in the adapting beam was rotated in 10° steps between horizontal orientations $\psi = [-90° + 90°]$. The log reflectance values were duplicated and one measurement was discarded to obtain 35 points of the standard PS display covering the full circle $\psi = [0 .. 350°]$. Individual ommatidial traces $A_m(\psi)$ were analysed in Fourier domain to obtain $\hat{A}_k$, where k is the frequency component ($k = 0$: DC response, $k = \pm 2$: modulation, $k = \pm 1$: empty fundamental). Relative modulation amplitude was obtained as $m = 2\,\mathrm{abs}(\hat{A}_2)/\hat{A}_0$ and the phase of maximal response was corrected as $\psi_{PS} = \arg(\hat{A}_2)/2$. We note that the relative modulation amplitude m is a linear parameter, different from the dichroic ratio or physiological PSR (polarisation sensitivity ratio): $PSR = (1 + m)/(1 - m)$.

Figure S1 – Stimulation protocols and bleaching

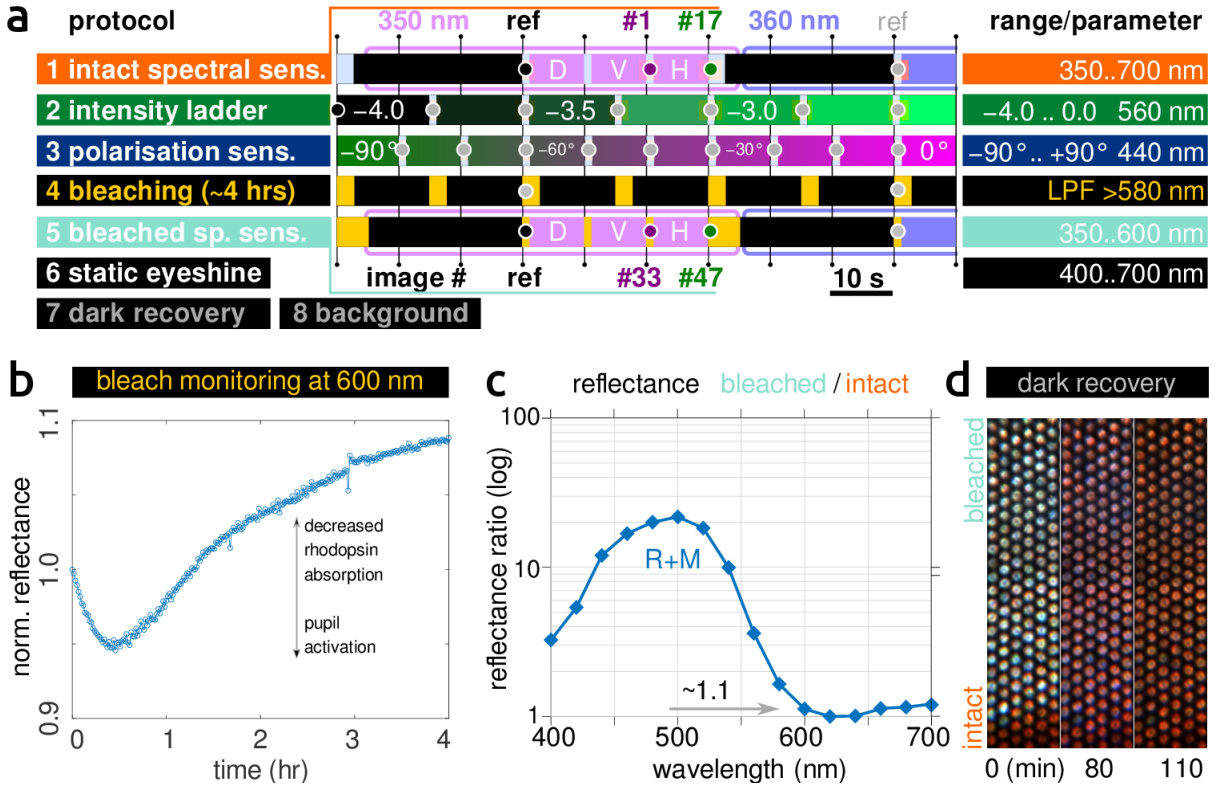

(a) Graphical description of the stimulation protocols. (1) Pupil spectral sensitivity of the intact eye was measured with adapting wavelengths in the range from 350 to 700 nm. At each adapting wavelength, four images were taken: first, the dark adapted reference, and then three images were taken after 10 seconds of linearly polarized adapting light with diagonal, vertical and horizontal orientations. **(2)** Intensity ladder was measured at 560 nm, with the adapting stimuli steps set to 0.25 log intensity by a combination of discrete ND filters and the ND wedge. **(3)** Polarisation sensitivity was measured at 440 nm, from H past V to H orientation in 10° steps. **(4)** While LED long-pass filtered above > 580 nm was used for bleaching. During every fourth bleach stimulus, an image at 600 nm was taken in order to monitor bleaching. **(5)** Pupil spectral sensitivity of the bleached eye was measured with adapting wavelengths in the range from 350 to 600 nm. LPF-filtered LED was used instead of the white LED. **(6)** Static eyeshine images were taken. **(7)** The eye was left to recover in the dark and a few colour images were acquired to document the process.

(b) Monitoring of bleaching. First, the normalized reflectance at 600 nm drops, probably due to slightly increased absorption by metarhodopsin and chronic activation of pupil. Then, as the metarhodopsin is being enzymatically removed and the visual pigment is depleted, the reflectance increases.

(c) Quantification of bleaching. A log reflectance difference spectrum between bleached and intact ommatidia, taken from the series of images shown in **Fig. 5a**, reveals that the reflectance around 500 nm (a wavelength close to the isosbestic point of green rhodopsin and its metarhodopsin), has increased ~20 times in the bleached ommatidia. This corresponds to one-pass peak absorbance change of ~0.65. Note also that the reflectance ratio at the test wavelength, 600 nm, is small, ~1.1 as in (b).

(d) Bleaching recovery. In the dark, the main green visual pigment is replenished and the orange tint of the eyeshine returns.

2. Fourier domain analysis of the ommatidial eyeshine

We analysed the dependence of the eyeshine radiation patterns at 600 nm on the intensity of green (540 nm) adapting light covering 4 log units of intensity. We selected a patch with 20×3 ommatidia and averaged the raw images in the Fourier domain. The eyeshine images were cropped so that the signal energy of 1D Fourier transform of each pixel column $g_{[y]}$ was maximally contained within the periodic components of $\hat{g}_k$, $k = 20i$, $i = 1, 2 \ldots$. The images were then resynthesised by admitting the DC component $\hat{g}_0$, the periodic components $\hat{g}_k$ and their first neighbours $[\hat{g}_{k-1}, \hat{g}_{k+1}]$ into the inverse 1D Fourier transform. Each resynthesised image thus contains three independent averages of 20 ommatidia, each in 20 copies that very slightly differ due to the lattice and pattern jitter. Three independent average radiation patterns were randomly selected for the analysis using circular/annular ROIs and transects.

Figure S2 – Extinction of waveguide modes due to pupil

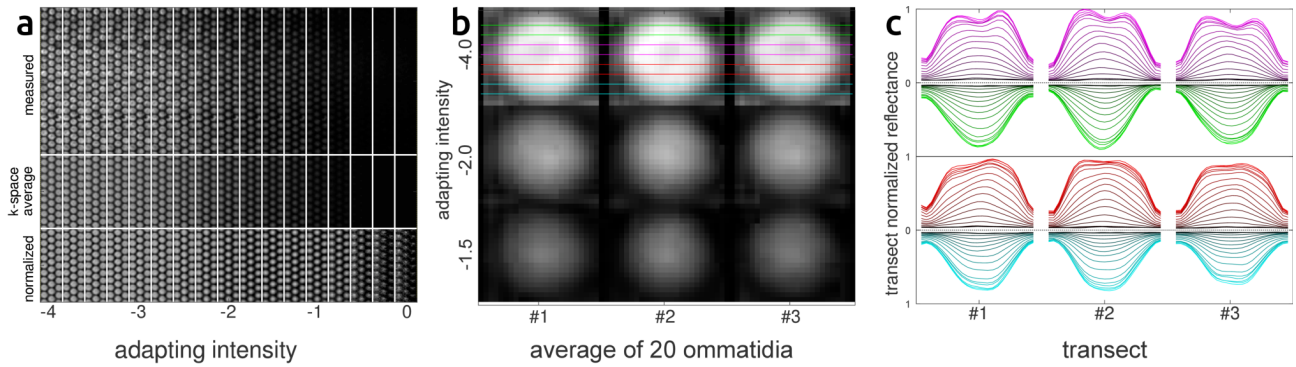

(a) Pupil response, seen as a reduction and narrowing of the reflected eyeshine patterns, is gradually becoming stronger over three magnitudes of adapting light. (a) The upper half of the montage is showing three columns of 20 ommatidia, taken at 600 nm after being adapted with 10 sec of green light (560 nm) of increasing intensities (*left to right*). (b) The lower half is showing images whose columns were averaged in frequency domain. In the bottom quarter, the individual images are normalized. The narrow spot reflections remaining at maximum adapting intensity are likely corneal lens reflections. **(b) Three magnified radiation pattern**s, each being a k-space average from 20 ommatidia, at three adapting intensities (dark adapted, -2, -1.5 log). The ROI transects used to produce the curves in (c) are delineated with coloured lines. **(c) Transects.** We analysed the difference in the attack of the pupil on the two waveguide modes with ROI transects. The reflectance of the patterns of (b) was averaged in areas between the lines with equal colour, magenta, green, red, and cyan, respectively. The resulting spatial profile through the pattern centre (*magenta, red*) of the dark-adapted state showed a depression which changed into a Gaussian-like curve at the more light-adapted state (*lines fading to black*). The intensity profiles of the transects through the pattern periphery (*green, cyan*) showed a similar shape at all adaptation states.

3. SVD decomposition and clustering of response spectra

The two matrices $M_{in}^{[628\times32]}$ and $M_{bl}^{[628\times28]}$ from the intact and the bleached spectral sensitivity runs contained ommatidial response spectra with area-normalized log-reflectance changes. The two matrices are shown side by side in **Fig. S3a**. Each part contains the pupil responses to VLP and HLP polarised stimuli. The two matrices were subjected to singular value decomposition as $M = UDV^T$, yielding a scaled spectrum matrix $S = DV^T$ and a scaled score (weights) matrix $W = UD$, where D is a diagonal matrix. The first few spectral components $S_{1..5}$ are shown in **Fig. S3c**. The component S_1 is corresponding to the averaged response of all ommatidia, which is in clearly higher for VLP adaptation stimuli in unbleached ommatidia. The component S_2 is contrasting the ultraviolet versus blue peak both in intact and bleached ommatidia. The scatter of score components $W_{2,in}$ and $W_{2,bl}$ are shown in **Fig. S3b**. The two components are highly correlated and show very clear grouping into three clusters, as seen by the marginal histograms. Classification into three ommatidial types was performed using k-means clustering of 8-dimensional score vectors composed from components $W_{2..5,in}$ and $W_{2..5,bl}$. Components $W_{1,in}$ & $W_{1,bl}$ were approximately constant due to normalisation and were not used for clustering. The three ommatidial classes, obtained with clustering, are shown in **Fig. S3d**. We infer from the curves that the distal photoreceptors R12 in the three classes are 2×blue (BB, *blue*), UV/blue (UB, *yellow*) and 2×UV (UU, *magenta*), respectively.

Figure S3 –Singular value decomposition and clustering